



HAL
open science

Lysine Trimethylation in Planktonic and Pellicle Modes of Growth in *Acinetobacter baumannii*

Nicolas Nalpas, Takfarinas Kentache, Emmanuelle Dé, Julie Hardouin

► **To cite this version:**

Nicolas Nalpas, Takfarinas Kentache, Emmanuelle Dé, Julie Hardouin. Lysine Trimethylation in Planktonic and Pellicle Modes of Growth in *Acinetobacter baumannii*. *Journal of Proteome Research*, 2023, 22 (7), pp.2339-2351. 10.1021/acs.jproteome.3c00097 . hal-04499889

HAL Id: hal-04499889

<https://hal.science/hal-04499889>

Submitted on 11 Mar 2024

HAL is a multi-disciplinary open access archive for the deposit and dissemination of scientific research documents, whether they are published or not. The documents may come from teaching and research institutions in France or abroad, or from public or private research centers.

L'archive ouverte pluridisciplinaire **HAL**, est destinée au dépôt et à la diffusion de documents scientifiques de niveau recherche, publiés ou non, émanant des établissements d'enseignement et de recherche français ou étrangers, des laboratoires publics ou privés.

1 Lysine trimethylation in planktonic and pellicle modes of growth in
2 *Acinetobacter baumannii*

3

4 Nicolas Nalpas^{1,#}, Takfarinas Kentache^{1,2,#}, Emmanuelle Dé¹ and Julie Hardouin^{1,2,*}

5

6 1. University of Rouen Normandie, INSA Rouen Normandie, CNRS, Polymers, Biopolymers,
7 Surfaces Laboratory UMR 6270, F-76000 Rouen, France

8 2. University of Rouen Normandie, INSERM US 51, CNRS UAR 2026, HeRacLeS-
9 PISSARO, Normandie Université, 76000 Rouen, France

10 # equal contribution

11

12

13

14 *Correspondence to:

15 Dr Julie Hardouin, Laboratoire Polymères, Biopolymères, Surfaces, UMR CNRS 6270,
16 Université de Rouen, 76821 Mont-Saint-Aignan cedex, France.

17 Tel: +33 (0)2 35 14 67 09

18 E-mail: julie.hardouin@univ-rouen.fr

19

20 **Keywords:** Lysine trimethylation, *Acinetobacter baumannii*, biofilm, proteomics, bacteria,
21 post-translational modifications.

22

23

24

25

26 **ABSTRACT**

27 Over the past 30 years, *Acinetobacter baumannii* has been described as an important
28 nosocomial pathogen due to frequent ventilator-associated infections. Many biological
29 processes of *A. baumannii* remain elusive, such as the formation of an air-liquid biofilm
30 (pellicle). Several studies demonstrated the importance of post-translational modifications
31 (PTM) in *A. baumannii* physiology. Here, we investigated K-trimethylation in *A. baumannii*
32 ATCC 17978 in planktonic and pellicle modes using proteomic analysis.

33 To identify the most high-confidence K-trimethylated peptides, we compared different sample
34 preparation methods (i.e. Strong cation exchange, antibody-capture) and processing software
35 (i.e. different database search engines). We identified, for the first time, 84 K-trimethylated
36 proteins, many of which are involved in DNA and protein synthesis (HupB, RplK), transporters
37 (Ata, AdeB) or lipid metabolism processes (FadB, FadD). In comparison with previous studies,
38 several identical lysine residues were observed acetylated or trimethylated, indicating the
39 presence of proteoforms and potential PTM cross-talks. This is the first large-scale proteomic
40 study of trimethylation in *A. baumannii* and will be an important resource for the scientific
41 community (availability in Pride repository under accession PXD035239).

42

43

44 INTRODUCTION

45 *Acinetobacter baumannii* is a nosocomial pathogen, member of the ESKAPE group of bacterial
46 pathogens (*Enterococcus faecium*, *Staphylococcus aureus*, *Klebsiella pneumoniae*, *A.*
47 *baumannii*, *Pseudomonas aeruginosa* and *Enterobacter* sp.)¹, responsible for a majority of
48 hospital-acquired infections. It has become an important human pathogen owing to both an
49 increasing number of infections and an emergence of multidrug-resistant (MDR) strains². *A.*
50 *baumannii* infections occur mostly in intensive care units and cause severe nosocomial
51 infections including pneumonia, bacteremia, endocarditis, skin and soft tissue infections,
52 urinary tract infections or meningitis^{3,4,5}. *A. baumannii* is known for its long-time survival in
53 hospital settings due to its great ability to survive desiccation⁶, oxidative stress⁷ or treatment
54 with disinfectants². This persistence is mostly linked to its capacity to form biofilms^{8,9}. Indeed,
55 MDR clinical isolates showed a high ability to form biofilm, which was positively associated
56 with a capability to adhere to human bronchial epithelial cells^{10,11}. *A. baumannii* can easily
57 form biofilms at the air-liquid (A-L) interface, usually named pellicles. In a previous study, we
58 showed that the *Acinetobacter* species forming pellicles are those mainly involved in
59 nosocomial infections such as *A. baumannii* and *A. nosocomialis*¹².

60 One research avenue to understand *A. baumannii* resistance and to find new ways of treatment
61 is to study post-translational modifications (PTMs). PTMs play a central role in bacteria since
62 they regulate protein functions essential for bacterial physiology, cell signaling and
63 environmental adaptation¹³. Furthermore, they enable increased protein versatility and allow
64 bacteria to respond rapidly to external signals.

65 Several proteomic studies have highlighted the diversity of modified proteins in *A. baumannii*.
66 O-linked protein-glycosylation can have a role in biofilm formation and virulence¹⁴. Serine,
67 threonine, and tyrosine phosphoproteomic investigations suggested that phosphorylation seems
68 to be important in *A. baumannii* resistance^{15,16}. Recently, the phospho-secretomes of two *A.*
69 *baumannii* strains, the reference strain ATCC 17978 and the virulent multi-drug resistant strain
70 AB0057, highlighted a higher number of phosphoproteins in the biofilm mode of growth
71 compared to the planktonic growth¹⁷. Moreover, five phosphosites were detected on the T6SS
72 tube protein Hcp¹⁷. After mutagenesis, specific phosphorylated residues were clearly shown to
73 be required for Hcp secretion and therefore T6SS activity. Lysine acetylation has also been
74 investigated in *A. baumannii* showing many acetylated proteins involved in various metabolic
75 processes, adaptation, virulence (iron acquisition pathways), biofilm formation, bacterial
76 virulence (*i.e.* in several iron acquisition pathways), or drug resistance¹⁸.

77 Trimethylation is an interesting PTM affecting lysine residues. It involves the successive
78 transfer of three methyl groups to the ϵ -amine of lysine residues by protein K-
79 methyltransferases (PKMTs)^{19,20}. This addition results in an increase in steric hindrance and in
80 the conservation of the positive charge of the lysine side chain²¹. Trimethylation can thus alter
81 protein-protein interactions and protein activity. As an example, a defect in histone
82 trimethylation regulation can lead to cancer in human²². Despite their importance, few large-
83 scale proteomic studies have been carried out on protein trimethylation characterization in
84 bacteria. In *E. coli*, in a quantitative proteomic study, 14 K-trimethylated proteins were
85 identified²³. These proteins were mainly involved in the protein biosynthesis pathway. In
86 *Rickettsia prowazekii*, the virulence factor OmpB contains more trimethylated lysines in
87 virulent strains compared to avirulent strains^{24,25}.

88 Our interest, in the present work, focuses on the K-trimethyl proteome profiles in *A. baumannii*
89 in two growth modes (planktonic and pellicle). In this context, we tested different sample
90 preparation methods to identify the optimal approach for the identification of K-trimethylated
91 peptides. We compared the processing of MS data using four database search engines to
92 prioritize the identifications of high confidence. We investigated the biological roles of K-
93 trimethylated proteins to highlight overrepresented functions and pathways. Finally, we
94 mapped the modified residues, observed here as well as in other studies, onto the three-
95 dimensional protein structures to understand the impact of these PTMs on the protein functions.
96 Our findings significantly deepen our knowledge of *A. baumannii* species and provide, to our
97 knowledge, the first resource of K-trimethylation for this opportunistic pathogen.

98
99

100 EXPERIMENTAL PROCEDURES

101 **Planktonic and pellicle growth conditions**

102 An overnight culture of *A. baumannii* strain ATCC 17978, performed in Mueller-Hinton Broth
103 (MHB, Difco), was used to inoculate 500 mL of MHB at a final concentration of 10^7 Colony
104 Forming Unit (CFU)/mL. For the planktonic growth, the culture was performed at 37°C under
105 a constant shaking for 24 h. Cells were harvested at the stationary phase of growth (*i.e.*, OD_{600} =
106 1.9), by centrifugation (2700 x g, 20 min, 4°C), and washed 3 times with deionized water. For
107 the pellicle formation, bacterial growth was performed in glass Erlenmeyer containing 500 mL
108 of MHB during 1-day or 4-days, without shaking, at 37 °C. Pellicles (1-day and 4-days) were
109 recovered from the surface of the culture, resuspended in 5 mL of a sterile phosphate buffered
110 saline solution (PBS, 10 mM, pH 7.4). Cell recovery from pellicles was performed by sonication
111 (twice during 15 min) and then by centrifugation (after each sonication at 4 000 x g, 15 min,
112 4°C). For each growth condition, the bacterial culture was performed in triplicate.

113

114 **Protein extraction**

115 Protein extraction from pellicle and planktonic samples were performed as described by Marti
116 *et al.* ²⁶ and Ouidir *et al.* ²⁷, respectively. Briefly, after centrifugation (2700 x g, 10 min, 4°C)
117 the resulting cell pellets were resuspended in 10 mL of Tris-HCl buffer (20 mM, pH 7.4).
118 Protease inhibitor cocktail (Protease Inhibitor Cocktail Set III, Sigma), and demethylase
119 inhibitors (1 mM of *trans*-2-Phenylcyclopropylamine, Sigma) were added. The mixtures were
120 sonicated twice, each for 3 min (Vibra Cell 75115, Bioblock Scientific). Unbroken cells were
121 eliminated by centrifugation (10 000 x g, 10 min, 4°C). An ultracentrifugation (60,000 x g, 45
122 min, 4°C) of supernatants allowed the isolation of cytoplasmic proteins. The protein
123 concentration was evaluated by the Bradford assay (Bio-Rad).

124

125 **Enzymatic digestion of protein extracts**

126 Twenty-five micrograms of proteins were mixed with SDS loading buffer (63 mM Tris-HCl,
127 pH 6.8, 10 mM DTT, 2% SDS, 0.02% bromophenol blue, 10% glycerol), then loaded onto a
128 SDS-PAGE stacking gel (7%). A short electrophoresis was performed (10 mA, 20 min) in order
129 to concentrate proteins. After migration, gels were stained with Coomassie Blue and destained
130 (50% ethanol, 10% acetic acid, 40% deionized water). The revealed protein band from each
131 fraction was excised, washed with water, and then immersed in a reductive medium (5 mM
132 DTT). Cysteines were irreversibly alkylated with 25 mM iodoacetamide in the dark. Following

133 washing steps in water, gel bands were submitted to protein digestion with trypsin (2 µg per
134 band), overnight at 37 °C, in ammonium bicarbonate buffer (10 mM and pH 8). Peptide
135 extraction was performed with H₂O/CH₃CN/TFA mixtures (49.5/49.5/1) and peptides were
136 then dried. Two technical replicates were carried out for each growth condition.

137

138 **Strong cation exchange chromatography**

139 Protein extract (3 mg) was solubilized in urea (6 M) and DTT (5 mM) during 30 min. Alkylation
140 of cysteines was performed with iodoacetamide (20 mM, 45 min). After a 4-fold dilution with
141 water, proteins were digested with trypsin (ammonium bicarbonate, pH 7.8, protein/trypsin
142 ratio: 1/100) overnight. FA 0.1% was added to the peptide sample to decrease the pH at 2.7.
143 Strong cation exchange chromatography was performed with a 1-ml Resource S column
144 (Amersham Biosciences). Peptides were separated with a linear gradient from 100% buffer A
145 (30% acetonitrile, 5 mM K₂HPO₄, pH 2.7) to 30% buffer B (30% acetonitrile, 5 mM K₂HPO₄,
146 350 mM KCl, pH 2.7) at a flow rate of 1 ml/min. Fractions were collected each mL and desalted
147 on C18 tip column according to the manufacturer's instructions. The eluates were dried and
148 frozen at -20 °C until further analysis.

149

150 **Sample preparation for enrichment of trimethyl-lysine peptides**

151 Proteins (3 mg) were solubilized in urea (8 M) and DTT (15 mM) during 1 h. The reduced
152 proteins were alkylated with iodoacetamide (20 mM, 45 min). Proteins were precipitated with
153 ice-cold acetone (-20 °C, 2 h). The protein pellet was resuspended in 1 mL of deionized water
154 and digested with trypsin (ammonium bicarbonate, pH 7.8, enzyme/protein ratio: 1/50 (w/w))
155 overnight at 37 °C. Peptides were dried and stored at -20 °C.

156 Peptides enrichment was performed following the manufacturer's instruction (PTM Biolabs
157 PTM-609). Sixty µL of anti-trimethyl-lysine polyclonal antibody conjugated to protein A were
158 washed three times with ice-cold PBS. The tryptic digest was redissolved in NETN buffer (100
159 mM

160 NaCl, 1 mM EDTA, 50 mM Tris, and 0.5% Nonidet P-40, pH 8.0), mixed with the conjugated
161 beads, and gently shaken at 4 °C for overnight. After incubation, the beads were carefully
162 washed three times with NETN buffer, twice with ETN buffer (100 mM NaCl, 1 mM EDTA,
163 and 50 mM Tris, pH 8.0). After water washes, beads were precipitated (8 000 x g, 1 min).
164 Trimethylated peptides were eluted 3 times with TFA 0.1% and desalted on C18 tip column.
165 Peptides were dried and stored at -20°C until prior to mass spectrometry analysis.

166

167 **Tandem mass spectrometry**

168 All experiments were performed on a LTQ-Orbitrap Elite (Thermo Scientific) coupled to an
169 Easy nLC II system (Thermo Scientific). One microliter of sample was injected onto an
170 enrichment column (C18 PepMap100, Thermo Scientific). The separation was performed with
171 an analytical column needle (NTCC-360/100-5-153, NikkyoTechnos, Japan). The mobile phase
172 consisted of H₂O/0.1% formic acid (FA) (buffer A) and CH₃CN/FA 0.1% (buffer B). Tryptic
173 peptides were eluted at a flow rate of 300 nL/min using a three-step linear gradient: from 2 to
174 40% B over 75 min, from 40 to 80% B in 4 min and 11 min at 80% B. The mass spectrometer
175 was operated in positive ionization mode with capillary voltage and source temperature set at
176 1.5 kV and 275 °C, respectively. The samples were analyzed using CID (collision induced
177 dissociation) method. The first scan (MS spectra) was recorded in the Orbitrap analyzer (R =
178 60,000) with the mass range m/z 400–1800. Then, the 20 most intense ions were selected for
179 MS² experiments. Singly charged species were excluded for MS² experiments. Dynamic
180 exclusion of already fragmented precursor ions was applied for 30 s, with a repeat count of 1,
181 a repeat duration of 30 s and an exclusion mass width of ± 5 ppm. Fragmentation occurred in
182 the linear ion trap analyzer with collision energy of 35 eV. All measurements in the Orbitrap
183 analyzer were performed with on-the-fly internal recalibration (lock mass) at m/z 445.12002
184 (polydimethylcyclsiloxane). The MS proteomics data have been deposited to the
185 ProteomeXchange Consortium *via* the PRIDE partner repository²⁸ with the data set identifier
186 PXD035239.

187

188 **Database searches**

189 Raw data files were processed using four different processing software packages: Proteome
190 Discoverer v. 1.4 (Thermo Scientific)²⁹, MaxQuant v. 2.1.4.0³⁰, FragPipe v. 18.0³¹ and
191 MetaMorpheus v. 0.0.320³². The peak lists were respectively searched using the search
192 engines: MASCOT (Matrix Science), Andromeda, MSFragger and Morpheus. The database
193 *Acinetobacter baumannii* ATCC 17978, containing 4097 protein sequences (Reference
194 Sequences: NC_009085.1, NC_009083.1 and NC_009084.1), was downloaded from
195 <http://www.genoscope.cns.fr>³³ and used for these searches. As much as possible, database
196 search parameters were kept identical between software and notably the following: 2 missed
197 trypsin cleavage sites allowed; variable modifications: carbamidomethylation of cysteine,
198 oxidation of methionine, deamidation of asparagine, lysine trimethylation and lysine
199 acetylation. The parent ion and daughter ion tolerances were 5 ppm and 0.35 Da, respectively.

200 False discovery rate (FDR) threshold for identifications was specified at 1% (for proteins and
201 peptides).

202

203 **Validation of trimethylated sites**

204 A number of filtering steps were implemented to strictly validate the trimethylated peptides
205 identified with the different processing software packages. Specifically, the threshold ion score
206 for PSM was ≥ 15 for Mascot, MetaMorpheus and FragPipe, while a score threshold of ≥ 50 was
207 used for MaxQuant. PSM with a posterior error probability below 0.05 were kept. Peptides with
208 trimethylation localized on the side chain of the last residue of the peptide sequence were
209 excluded (except if the modification occurred on the last residue of the protein sequence)
210 because trypsin cannot cleave after a modified lysine. Finally, all MS/MS mass spectra were
211 manually checked to ensure the quality of the peptide sequence and the modified site
212 annotation. In a few cases, annotation conflicts were observed (between software or similarly
213 ranked matches) and the following rules were implemented to decide: (1) the sequence
214 annotation with the least number of modifications was favored; (2) for conflict between
215 carbamidomethylation (C) and trimethylation (K) + oxidation (M), the sequence with
216 carbamidomethylated cysteine were privileged as it is usually considered a fixed modification;
217 (3) for conflict between acetylation (K) and trimethylation (K), the acetylated lysine were
218 retained as this modification is more frequent in bacteria; (4) the sequence annotation that was
219 identified by a maximum number of software was kept. The trimethylated peptides that did not
220 pass all above criteria were removed and are not discussed in this study.

221

222 **Retrieval of protein functions**

223 For each protein sequence, the reciprocal best hit method ³⁴ was used to obtain the
224 corresponding unique accession identifier in different web resources, namely GenBank (*i.e.*
225 A1S_XXXX), UniProt (*i.e.* 6 or 10 alphanumeric characters), VFDB (*i.e.* VFCXXXX) and
226 CARD (*i.e.* ARO:XXXX). Notably, this allowed the retrieval of protein cellular localization
227 (<http://www.genoscope.cns.fr>), Gene Ontology functional categories (UniProt), canonical
228 pathways (KEGG), virulence (VFDB) and resistance (CARD) information.

229 The InterProScan v. 5.55-88.0 software ³⁵ was used for protein sequence analysis in order to
230 identify functional domains and conserved sites. The eggNOG-mapper v. 2.1.8 software ³⁶ was
231 used on the protein entries from *A. baumannii* to retrieve functional annotation (COG
232 categories) based on orthology ³⁷.

233 To understand the context of trimethylated sites within secondary protein structures (coil, helix,
234 sheet), we predicted them using the NetSurfP-3.0 software ³⁸. The trimethylated sites were then
235 summarized (e.g. count, proportion) based on their location within different protein surface
236 accessibility areas and secondary structures.

237

238 **Bioinformatic analyses**

239 The rmotifx R package ³⁹ was employed to determine the presence of characteristic motifs
240 within trimethylated peptide windows (31 residues). Trimethylated sites were selected for the
241 overrepresentation analysis based on their central residue (i.e. K) and tested against a
242 background of all K-modified sites identified in this study (p -value ≤ 0.01 and sites count ≥ 5).
243 The clusterProfiler package ⁴⁰ based on hypergeometric distribution (adjusted p -value ≤ 0.05)
244 was used to test for overrepresentation of functional categories within different protein set (sites
245 identified in pellicle, in planktonic, in common, etc).

246 The protein three-dimensional structures were also searched with the online software Alphafold
247 (<https://alphafold.ebi.ac.uk/>) ⁴¹ or RCSB Protein Data Bank (<https://www.rcsb.org>) ⁴². When
248 the structure was not referenced, protein alignments were performed to check for
249 proteins/residues conservation with NCBI BLAST (<https://blast.ncbi.nlm.nih.gov/Blast.cgi>) ⁴³.
250 The custom visualization of protein 3D structure was done with PyMOL (<https://pymol.org/2/>),
251 notably to display multiple PTMs per structure.

252

253 RESULTS AND DISCUSSION

254 We investigated K-trimethylations in *A. baumannii* ATCC 17978 strain in planktonic and
255 pellicle modes of growth. The trimethylated peptides are present in sub-stoichiometric levels,
256 thus we implemented different sample preparation to detect these peptides. Notably, we
257 prepared for measurement standard digested samples, samples fractionated with strong cation
258 exchange (SCX) and samples treated with anti-trimethyl-lysine antibodies for affinity capture.
259 All MS analyses were performed on a high accuracy and high-resolution mass spectrometer
260 ($\Delta m \leq 5$ ppm) in order to differentiate between acetyl-lysine and trimethyl-lysine, which have
261 close masses (42.011 Da versus 42.047 Da, respectively). Subsequently, we used four different
262 search engines to identify the K-trimethylated peptides. We then compared the search results
263 and used stringent filtering parameters to maximize the quality of our identifications. We will
264 initially present the findings of the search engines comparison and then discuss the results of
265 the different sample preparation approaches.

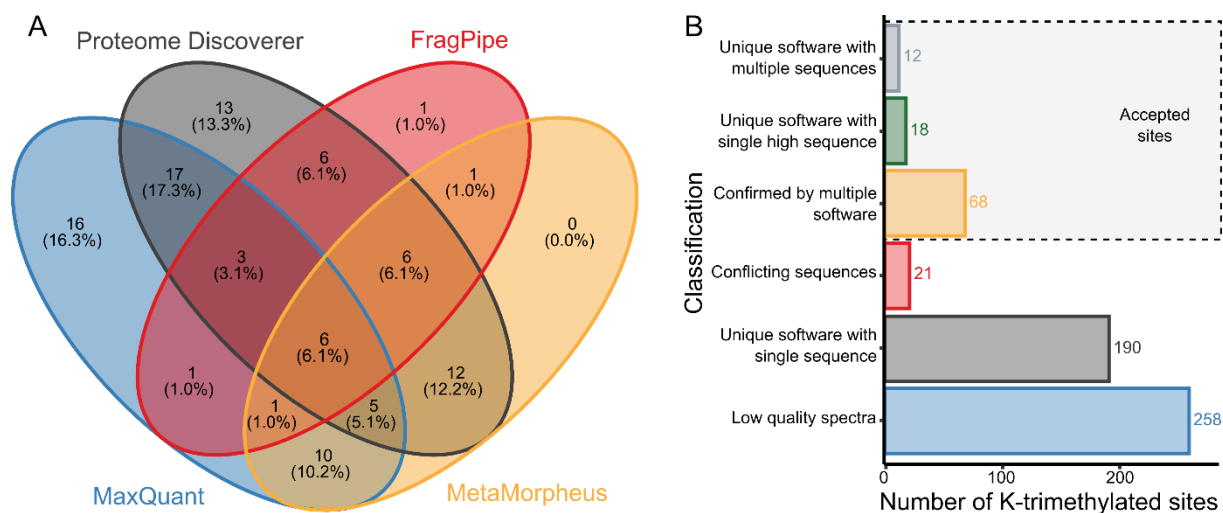
266

267 **Manual validation of MS/MS spectra is necessary for extended combination of** 268 **modifications**

269 We used four database search engines, namely Proteome Discoverer ²⁹, MaxQuant ³⁰,
270 MetaMorpheus ³² and FragPipe ³¹ in order to identify the K-trimethylated peptides and
271 associated proteins. Based on the trimethylated sites, this strategy resulted in a very poor
272 identification overlap (1.1%) between all software packages. Indeed, 81.1% of trimethylation
273 were identified by a single software (Figure S1A). A majority of sites were also identified based
274 on a single peptide spectrum match (PSM) (Figure S1B). Together these results point to a
275 potentially high number of false positive hits, or at least hits of poor quality.

276 In this context, we manually verified the best MS/MS spectra of each trimethylated peptide that
277 passed our initial filtering quality criteria ($n = 567$). This manual assessment resulted in 98
278 trimethylated sites (corresponding to 84 trimethylated proteins) in the final list. Of which, 16,
279 13, 1 and 0 sites were uniquely identified by MaxQuant, Proteome Discoverer, FragPipe and
280 MetaMorpheus, respectively. Thus, the percentage of sites identified by a single software was
281 reduced to 30.6% and is indicative of an improved dataset (Figure 1A). For the sites that were
282 not retained, the majority were of low quality based on our manual review of MS/MS spectral
283 annotation (Figure 1B). For the rest of this study, we only considered the 98 sites that passed
284 our stringent filtering and thus combined the identifications from the different search engines.

285



286
 287 **Figure 1: Combination of multiple search engines and filtering criteria to identify K-**
 288 **trimethylated peptides.** (A) Numbers of K-trimethylated sites identified using different
 289 database search engines and after manual validation of MS/MS spectra. (B) Number of K-
 290 trimethylated sites that passed (or not) the stringent filtering criteria.
 291

292 **SCX fractionation provides the most identification of K-trimethylated sites**

293 The digested sample was, first, analyzed by nLC-MS/MS without any sample prefractionation
 294 or enrichment approaches. With this approach, only 7 K-trimethylated sites were identified
 295 irrespective of the mode of growth (Figure 2A, Table S1).

296 To improve trimethylated peptide characterization, we decided to use affinity chromatography
 297 with anti-trimethyl-lysine antibodies. No proteomic studies of samples enriched *via* these
 298 antibodies have been published to our knowledge. We only identified 5 sites through this
 299 enrichment method (Figure 2A, Table S1), which demonstrates the poor efficiency of these
 300 antibodies to capture K-trimethylated peptides.

301 The third approach tested consisted in pre-fractionation of peptides with SCX. In this context,
 302 SCX was the best approach to identify K-trimethylated peptides. Indeed, 98 K-trimethylated
 303 sites were identified via SCX, which included the sites found with the other two approaches
 304 (Figures 2A, Tables S1).

305 We also checked whether the trimethylated sites were also identified in mono- and dimethylated
 306 states as trimethylation is rarely thought to occur without lower methylation state among
 307 eukaryotes. To do so, we searched the MS data with inclusion of these two additional variable
 308 modifications. Our results showed that 36 trimethylated sites were also mono- or dimethylated
 309 (Table S1). It should be noted that other global K-methylation studies obtained similar overlap
 310 between methylation state at specific sites^{44,45}.

311 We then used the NetSurfP software to predict the proteins secondary structures and solvent
 312 accessibility in order to check whether the trimethylated sites were located on accessible

313 residues and thus can be enzymatically added. Here, the K-trimethylated residues are in their
314 majority (92.8%) localized within exposed regions of the protein secondary structure, with
315 median relative solvent accessibility (RSA) of 0.57 (Figure S2A-B). Similar results have been
316 reported in the context of phosphorylation ^{46,47} and provide an additional layer of confidence
317 regarding the modified sites reported here.

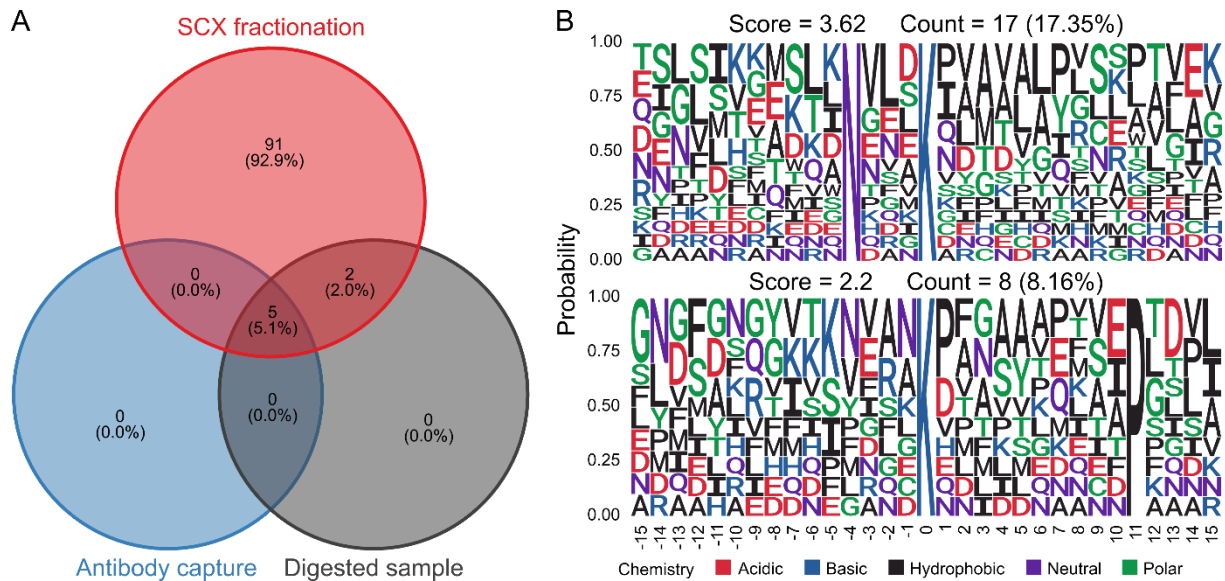
318

319 **Conserved residues surrounding the trimethylated lysine for recognition by protein K-** 320 **methyltransferases**

321 In the future, it will be important to understand which specific PKMTs and demethylases are
322 adding and removing methyl groups on specific protein substrates. However, few PKMTs are
323 known in *A. baumannii* or bacteria in general and it is not clear if they are responsible for
324 trimethylation addition. For example, PrmA (A1S_2184) and PrmB (A1S_1693) of *A.*
325 *baumannii* transfer methyl group on the 50S ribosomal subunit protein L11 and L3, respectively
326 ²⁰. The few other interesting bacterial PKMTs include the protein EF-Tm which targets EF-Tu
327 as reported in *P. aeruginosa* ⁴⁸, the protein FliB which catalyzes a [4Fe-4S] mediated methyl
328 transfer reaction on flagellin of *Salmonella enterica* ⁴⁹. To our knowledge, there are no known
329 demethylases in bacteria.

330 One strategy to understand which substrate are recognized by PKMTs consists in finding
331 substrate sequence motifs. Here, we tested for amino acid sequence motif enrichment in the
332 surrounding of the trimethylated sites (Figure 2B). Two substrate motifs were significantly
333 enriched (p-value < 0.01), even though there are few candidate sequences corresponding to each
334 motif. We highlighted the presence of Asparagine at position -4 (17.4% of all trimethylated
335 sequences) and Proline at position +11 (8.2%). These motifs fit with a previous study on the
336 parasite *Plasmodium falciparum* ⁴⁵, which shows K-trimethylated sequence motif to be
337 overrepresented with Asparagine. To our knowledge, we propose here the first consensus motifs
338 for K-trimethylation in bacteria.

339



340

341 **Figure 2: The optimal laboratory approach to identify K-trimethylated peptides.** (A)
 342 Numbers of K-trimethylated sites identified based on different analytical approaches and
 343 irrespective of the growth modes. (B) Over-represented sequence logos for the amino acid
 344 window (± 15 residues) around K-trimethylated sites (p -value < 0.01).
 345

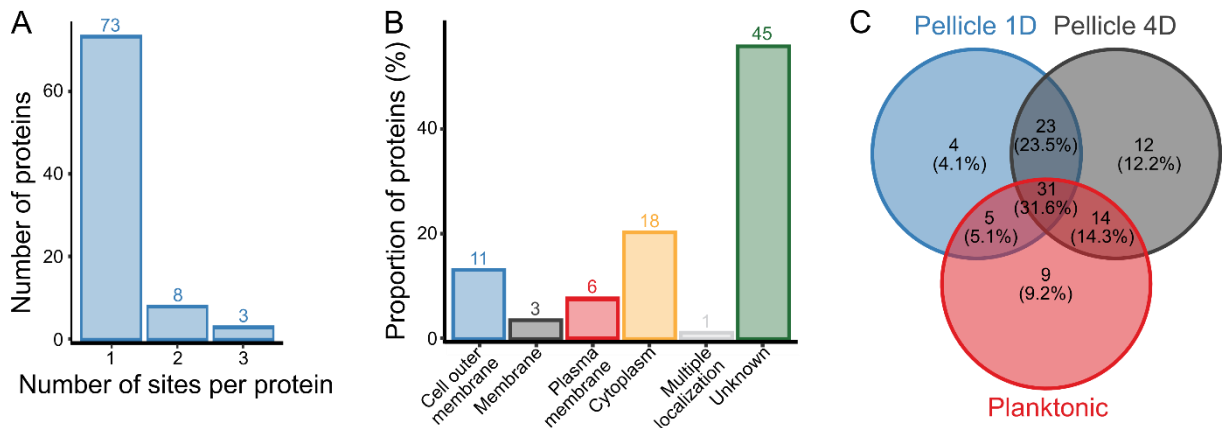
346 **More K-trimethylated proteins were identified in *A. baumannii* during pellicle growth
 347 mode**

348 Together, these approaches allowed us to identify 84 K-trimethylated proteins. In our previous
 349 study of K-acetylation in *A. baumannii*¹⁸, we found that 6.8% of all proteins were acetylated,
 350 which is significantly more than the 2.1% of trimethylated proteins identified here. The majority
 351 of K-trimethylated proteins (87%) have only one modified site (Figure 3A). Three proteins were
 352 found with three trimethylation sites: the protein 50S ribosomal protein L11 (RplK), the
 353 electron transfer flavoprotein beta subunit protein (EtfB) and the potassium binding protein
 354 Kbp. Another eight proteins harbored two modified lysine residues (Table S1), for example
 355 DnaK, GroEL and EF-Ts.

356 The majority of the K-trimethylated proteins were of unknown (47.9%) or cytoplasmic (17.3%)
 357 localization (Figure 3B). We then specifically examined trimethylated sites according to the
 358 growth modes in which they were identified (Table S2). The numbers of modified sites were
 359 similar between the three modes of growth (planktonic, pellicle 1 day and pellicle 4 days).
 360 However, only 31 sites, corresponding to 26 proteins, were found in common (Figures 3C and
 361 Table S2). Among these proteins were the 50S ribosomal protein L11 (RplK), the potassium
 362 binding protein (Kbp), Cu(+) exporting P-type ATPase (CopA), the transcriptional activator
 363 protein (AnoR), the electron transfer flavoprotein subunit beta (EtfB), an integrase (A1S_1175)
 364 as well as the signal recognition particle receptor (FtsY). Five conserved proteins of unknown

365 function were also common to all growth modes and worth investigating in the future
 366 (A1S_2027, A1S_2230, A1S_3626, A1S_3013 and ABYAL1975). In this context, these
 367 common trimethylation events are not specific to any growth mode and likely participate within
 368 core biological mechanisms. Interestingly based on our previous study⁵⁰, we observed that
 369 nearly half of the K-trimethylated proteins were also significantly changing in abundance
 370 between the different growth modes (n = 41) (Figure S3).

371



372

373 **Figure 3: The repartition of K-trimethylated proteins in terms of cellular localization and**
 374 **growth modes.** (A) The number of proteins identified with a single or multiple K-trimethylated
 375 sites. (B) The proportion of K-trimethylated proteins classified per cellular localization. (C)
 376 Numbers of K-trimethylated sites identified based on the different growth modes: pellicle 1
 377 day, pellicle 4 days and planktonic.

378

379 **K-trimethylated proteins were distributed across all biological functions**

380 The majority of proteins on which trimethylation was detected have an unknown function
 381 (Figure S4A). Other highly represented functions were “Energy production and conversion”
 382 and “Nucleotide metabolism and transport”. Interestingly, some functional categories displayed
 383 an increased representation between planktonic and pellicle modes, such as “Coenzyme
 384 metabolism”, “Translation” and “Post-translational modification, protein turnover, chaperone
 385 functions” (Figure S4A).

386 We retrieved gene essentiality information from the OGEE database⁵¹. Based on these data,
 387 14.3% of the protein-coding genes (*i.e.* 599 genes) are essential in *A. baumannii*. This reveals
 388 an over-representation in our dataset since 33% of the genes encoding for the K-trimethylated
 389 proteins are essential (28 genes) (Figure 4A and S4B). We will now discuss some key proteins
 390 for *A. baumannii* pathogenesis and metabolism, on which trimethylation was found (Figures
 391 4A and 5).

409 eubacteria and condenses DNA. Here, we identified HupB trimethylated on K38 (Figure 4B
410 and 5). In our previous study, it was acetylated on N-term (position 2) and on the five lysines
411 K3, K13, K23, K64 and K72¹⁸. In *Clostridium acetobutylicum*, K38 of HU orthologue was also
412 acetylated⁵³. HU orthologues can be modified by different PTMs, as recently summarized⁵².
413 These PTMs, such as the trimethylated K38, are located in predicted regions of direct
414 interactions with DNA at the top of the dimeric structure. The steric hindrance due to
415 trimethylation can therefore impact the protein/DNA interactions.

416 The transcriptional activator protein, AnoR (aka. AbaR) protein, is part of the LuxR family of
417 transcriptional regulators, although it is not clear whether it forms a dimer as observed for other
418 members of this family⁵⁴. This family plays a key role in bacterial quorum sensing. Notably,
419 AnoI (AbaI) is responsible for the synthesis of the quorum sensing signal N-(3-hydroxy-
420 dodecanoyl)-L-homoserine lactone (OH-dDHL), which binds to its receptor AnoR resulting in
421 its activation⁵⁵. AnoR is then able to regulate the expression of many genes (via recognition of
422 *lux* boxes) that are involved notably in motility and biofilm formation⁵⁴. This protein was
423 trimethylated on K225 that is situated within the DNA-binding domain, which allows
424 recognition of gene targets by AnoR.

425 The RNA polymerase subunit β' (RpoC) belongs to the RNA polymerase core enzyme, which
426 controls the transcription process. Specifically, the subunit β' (together with subunit β) is
427 important for interaction with the σ factors (recognition of promoter) and DNA template⁵⁶. In
428 *B. subtilis*, a mutation in *rpoC* resulted in increased activity of σ factors and ultimately in the
429 resistance to cephalosporin⁵⁷. Here, this protein was trimethylated on K238 and K1259, which
430 are respectively within the RNA polymerase domain 1 and 5. In other published studies, it was
431 acetylated on K10, K55, K65 and K79¹⁸ and phosphorylated on S37¹⁶. Interestingly, all
432 acetylated and phosphorylated residues are located within the clamp domain, which contribute
433 to the positioning of DNA and nascent RNA polymers.

434

435 Protein synthesis and folding

436 In addition to the proteins implicated in DNA metabolism, we identified many actors involved
437 in protein synthesis (i.e. RplK, EttA, EF-Ts, LepA) and folding (i.e. DnaK, GroEL, GroES,
438 FtsY) that were trimethylated (Figure 5).

439 L11 (RplK) is a conserved ribosomal protein and is situated at the base of the L7/L12 stalk of
440 the ribosome (50S subunit). It is required for the binding of several translational GTPases,
441 translational factors and the 23S rRNA. It plays a role during initiation, elongation and

442 termination of protein synthesis⁵⁸. Here, RplK was found trimethylated on K4, K17 and K40
443 in all growth modes (Figure 5). It was previously described as trimethylated in *E. coli* on K4
444 and K40^{59,60} and in *Thermus thermophilus*, on K17 and K40⁶¹. These modified sites are thus
445 likely conserved across bacteria. Importantly, the modified sites are located within the N-
446 terminal domain, which is implicated in direct ribosome-factor contacts, such as EF-G and EF-
447 Tu⁶², and in the regulation of the activity of (p)ppGpp synthetase I (RelA), an important protein
448 for stringent response^{63,64}. This domain is also a partial target for the antibiotic thiostrepton,
449 which stimulates the biofilm formation as well as inhibits the growth of clinical isolates of *P.*
450 *aeruginosa* and *A. baumannii*⁶⁵.

451 The protein EttA is also important for the protein synthesis initiation. Indeed, in presence of
452 high concentration of ATP, EttA will allow the formation of the first peptide bond by the
453 ribosome, which can enter the elongation phase. However, in cells lacking energy (high ADP
454 concentration), the initiation of the elongation cycle cannot start⁶⁶. EttA was found
455 trimethylated on K180 within an AAA+ ATPase domain and just outside of an ABC
456 transporter-like conserved region (Figure 5). Based on the 3D structure prediction of this
457 protein, the lysine at position 180 (or K192 for AlphaFold A0A0E1PLS2 protein) is located
458 within a coil region and seems to interact with W139 (or W147 for AlphaFold A0A0E1PLS2
459 protein). Of note this tryptophan is the last amino acid of the second α -helix constituting the
460 conserved linker region, which participates in the tRNA interaction⁶⁷.

461 Upon entry in the elongation cycle, the protein chain elongation factor EF-Tu will transport
462 aminoacylated tRNAs to the ribosome. To do so, it will form a complex with EF-Ts (Tsf)⁶⁸
463 that specifically drives the exchange of GDP by GTP during the peptidyl transfer⁶⁹. During
464 pellicle growth, EF-Ts was trimethylated on lysines 25 and 52 (Figure 5 and S5). Interestingly,
465 both of these modified sites are situated in the UBA-like domain, which is known to be involved
466 in ubiquitin-binding and proteasomal degradation⁷⁰. The two modifications could therefore
467 regulate the recognition of EF-Ts targets. Interestingly, EF-Ts was observed acetylated (N-term,
468 K213, K228) and phosphorylated (T2, T5, S7 and S211) in published studies^{16,18}. Based on the
469 crystal structure of the EF-Tu/Ts complex in *E. coli*, the N-terminal region as well as residue
470 K52 (K51 in *E. coli* - P0A6P1) are critical for the interaction with EF-Tu⁶⁸. In addition, the
471 residues 180-228, as well as the tip of the helical hairpin (204-208), constitute the dimerization
472 domain between two EF-Ts.

473 Following the elongation step, EF-G will perform ribosome translocation so that the next codon
474 can be decoded. Unlike other elongation factors, LepA has the ability to back-translocate the
475 tRNAs on the ribosome. This function is carried out upon mistranslocation of the ribosome and

476 will result in a second attempt for accurate translocation ⁷¹. LepA is conserved among bacteria
477 and allows accurate and efficient protein synthesis. This protein was trimethylated (K561) only
478 in pellicle growth. Previously, two lysine residues were also observed acetylated (K228 and
479 K231). Interestingly, the trimethylation is located within the LepA specific C-terminal domain,
480 which was proposed to be responsible for the presence of LepA in the periplasmic membrane.
481 Following protein synthesis, chaperones will fold newly synthesized proteins into their tertiary
482 structure. The protein DnaK (the bacterial equivalent of Hsp70) contributes to protein refolding
483 following stress incidents and captures protein aggregates forming upon antibiotic treatment.
484 Also, DnaK is known for its involvement in antibiotic resistance in *A. baumannii* ^{72,73}. DnaK
485 was found trimethylated on K252 and K269 (or K262 and K279 for AlphaFold A0A0E1Q1U0
486 protein) during pellicle growth (Figure 5). Both residues are located within the ATPase domain
487 and more specifically in the subdomain IIB. Importantly, several residues of this subdomain are
488 important for the recognition and binding of nucleotide exchange factors ⁷⁴. In our previous
489 study, this protein was acetylated on K83, K165, K182, K303, K320, K351 and K533 ¹⁸.
490 The GroEL-GroES complex plays a key role in protein folding ⁷⁵ and comprises two heptameric
491 rings of GroEL (forming a cavity) and a heptameric ring of GroES (acting as a lid). Unfolded
492 substrate proteins will be able to enter the cavity and upon ATP hydrolysis will be folded before
493 being released ⁷⁶. Importantly, it has been shown that upon over-expression this complex
494 promotes tolerance to aminoglycoside antibiotics in *E. coli* ⁷⁷ and *A. baumannii* ⁷⁸. The
495 chaperonins GroEL and GroES were trimethylated on K142 and 207, and K35, respectively.
496 GroEL was found acetylated on K34, K117 and K528 in our previous study ¹⁸ whereas GroES
497 is reported phosphorylated on S2, D9 and H8 in the dbPTM resource ⁷⁹. The extensive
498 modifications of chaperones (i.e. DnaK and GroEL) have already been reported in bacteria (i.e.
499 *Leptospirillum*) ⁸⁰.
500 FtsY allows the sorting of newly synthesized protein to the endoplasmic reticulum and plasma
501 membrane ⁸¹. This protein associates with the membrane and interacts with SecYEG (protein-
502 conducting channel) ⁸². This will result in the activation of FtsY, which will function as a
503 receptor for the SRP and ribosome-nascent chain ⁸¹. The ribosome-nascent chain is then
504 transferred to its final cellular localization. FtsY was reported acetylated (K69) and
505 phosphorylated (T23) within the SRP receptor domain in published works ^{16,18}. Here, it was
506 trimethylated on K261, which is located within an α -helix of the AAA+ ATPase domain. This
507 lysine is predicted to interact with E304 from another α -helix. Due to its location within the
508 protein, the trimethylation may have an effect on steric hindrance and thus disrupts ATP binding
509 and hydrolysis.

510 These trimethylation events may regulate the structural conformation, the interaction with
511 partners or the final localization of their respective proteins.

512

513 Drug efflux pumps, porins and transporters

514 Several protein families are embedded in the plasma or outer membranes of *A. baumannii* and
515 are of special importance in the context of virulence and antibiotics resistance, such as drug
516 efflux pumps or iron transporters⁸³ (Figure 5).

517 The DcaP-like protein (A1S_1380) has a porin domain and is located on the cell outer
518 membrane. It was shown in the AB307-0294 strain that DcaP was the most expressed diffusion
519 channel in the mouse model infected with this bacterium⁸⁴. In addition, this protein displayed
520 a reduced abundance in carbapenem-resistant *A. baumannii*⁸⁵. For these reasons, this protein is
521 considered as a candidate for vaccine development in *A. baumannii*⁸⁶. DcaP forms a trimer and
522 allows the uptake of carboxylic acids. This specificity has been used for the import of
523 antibiotics, such as sulbactam^{84,85}. Here, K56 was trimethylated only in pellicle modes (Table
524 S1). Based on the structure of DcaP in *A. baumannii* (X-ray crystallography), the residue 56 is
525 located in the disordered region of the extended coiled-coil N-terminus domain. The latter likely
526 contributes to the stability of the trimeric channel⁸⁴. Another hypothesis is that the N-terminus
527 region of DcaP functions as a substrate selection gate, as observed for the CymA porin⁸⁷. In
528 this context, the trimethylation could either block or increase the interaction between monomers
529 or participate in substrate-selection.

530 Aerobactin siderophore receptor IutA (A1S_1655) harbors a TonB-dependent outer membrane
531 receptor domain. The action of this receptor is unclear, but it seems to be involved in iron uptake
532⁸⁸. Previously, this protein was found significantly changing in abundance in pellicle 4-days³⁴.
533 In experiments using *Yersinia pseudotuberculosis*, this protein was knocked-out and displayed
534 reduced virulence and biofilm formation⁸⁹. Interestingly, this protein has been evaluated for
535 the development of a vaccine, with 50% survival rate after immunization in mice model of
536 infection by *A. baumannii*⁹⁰. Here, this protein was trimethylated on K13. This residue is within
537 the N-termini as observed for DcaP and may have a similar functional effect.

538 We identified two proteins that were trimethylated and part of the ABC transporters family: the
539 glutamate/aspartate ABC transporter periplasmic binding protein GltI (K286) and the putative
540 ABC transporter ATP-binding protein YbbA (K121). GltI was identified with K-acetylation in
541 our previous study although on a different lysine residue (K165)¹⁸. Interestingly, YbbA belongs
542 to MacB-like ABC transporters but does not form tripartite pumps and seems to be involved in

543 lipoprotein export. MacB-like ABC transporters have been shown to be essential for drug
544 resistance in cyanobacterium ⁹¹. The trimethylated residue of YbbA is within the MacB-like
545 ATP-binding domain.

546 The multidrug RND efflux pump AdeB is a transporter belonging to the AdeABC efflux
547 system. The structure and role of this complex has been extensively described elsewhere ⁹².
548 This protein has been reported for its involvement in antibiotic resistance, notably its
549 overexpression confers resistance to tigecycline ⁹³. The deletion of the gene *adeB* resulted in
550 reduced biofilm formation ⁹⁴. Here, we found this protein trimethylated on K776 (Figure 5 and
551 S5), which is located within an α -helix in the docking domain. As observed in a previous study,
552 the docking domain is rich in residues that are important for direct contact with AdeA ⁹². Due
553 to its localization, this modification may thus impact the interaction between AdeA and AdeB.
554 It is also possible that the trimethylation has an effect on interaction with the substrates, as the
555 deep binding pocket is in close proximity ⁹⁵.

556 The adhesin Ata is a trimeric autotransporter and a known virulence factor in *A. baumannii*.
557 This protein is required for adhesion and invasion of human endothelial and epithelial cells ⁷⁰,
558 notably by being able to bind to host glycans, such as galactose and *N*-acetylglucosamine ⁹⁶. It
559 was also shown to induce apoptosis following infection of human umbilical vein endothelial
560 cells by *A. baumannii* WT versus Δ *ata*. This protein was found trimethylated on K1020 and
561 acetylated on K1607 in our previous study ¹⁸ (Figure 5). The trimethylated site is located in a
562 helix region of the protein, based on the SwissModel (but of low confidence). This lysine can
563 be in interaction with D1024. However, due to the lack of structural information it is unclear
564 where this residue is located in a trimeric organization and whether it could impact
565 oligomerization or recognition of host glycans.

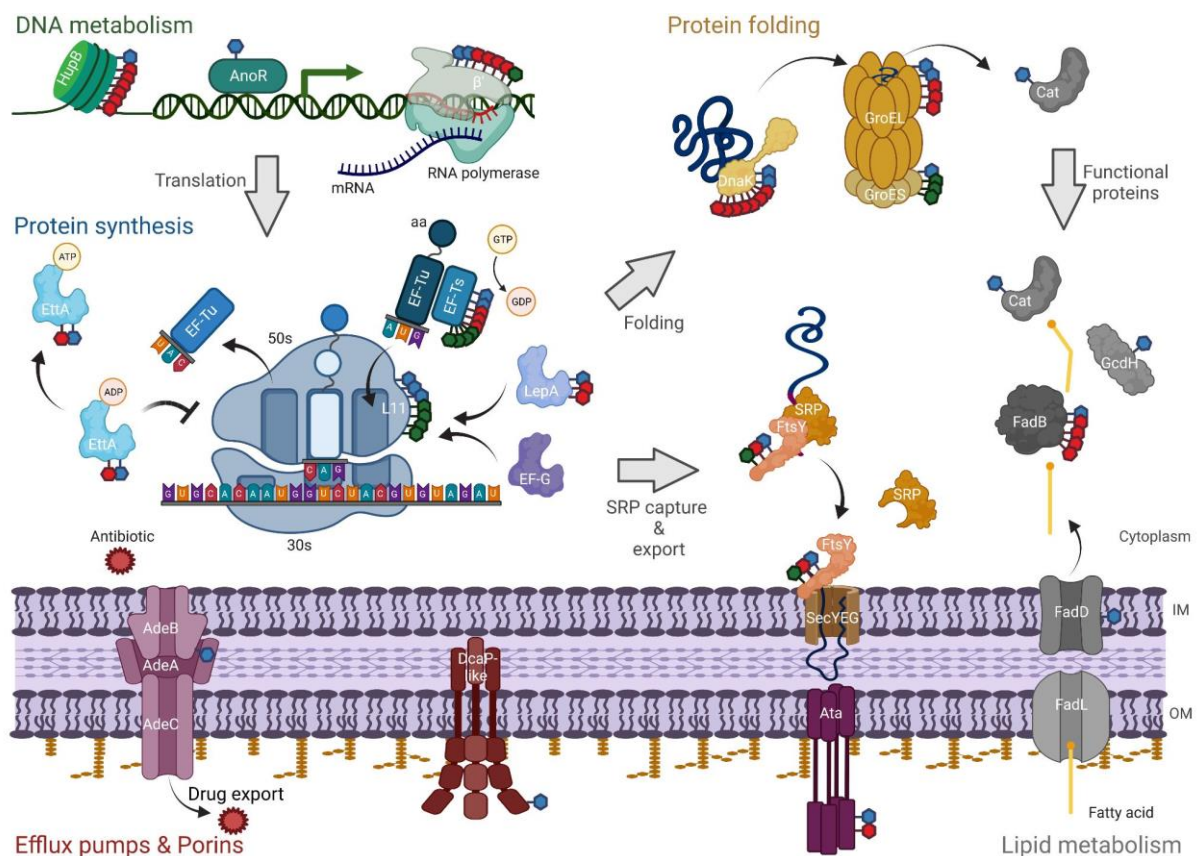
566

567 Lipid transport and metabolism

568 Lipids are important components of the bacterial membrane. The biosynthesis and degradation
569 pathways of fatty acids are therefore constantly being triggered. In addition, the degradation of
570 fatty acids has been shown to protect *A. baumannii* against the antibacterial activity of host-
571 produced long-chain polyunsaturated fatty acids ⁹⁷. In our dataset, five proteins involved in lipid
572 transport and metabolism were identified trimethylated: FadB, FadD, Cat, GcdH and a
573 conserved protein of unknown function (A1S_3626) (Figure 5).

574 The Succinyl-CoA:coenzyme A transferase (Cat) and Glutaryl-CoA dehydrogenase (GcdH)
575 were, respectively, trimethylated on K74 and K175. We will not expand further on these

576 proteins since little has been reported in the literature, besides their potential involvement in β -
 577 oxidation pathway⁹⁸. FadD (inner membrane) and FadB (cytoplasm) allow the transport of long
 578 chain fatty acids into the cytoplasm and the conversion of enoyl-CoA to 3-ketoacyl-CoA as part
 579 of the β -oxidation cycle, respectively⁹⁹. Here, the long-chain-fatty-acid-CoA ligase FadD and
 580 the fatty acid oxidation complex subunit alpha FadB proteins were trimethylated on K493 and
 581 K77, respectively (Table S1). K77 of FadB (or K244 of B2I2J9 – UniProt) is found within the
 582 ClpP/crotonase-like domain, which controls enolate and oxyanion reactivity¹⁰⁰. Interestingly,
 583 FadB was found acetylated on K77 and on 3 others lysines (K52, K203 and K430) as well as
 584 phosphorylated (S363) in other published works (Figure S5)^{16,18}. With the exception of K52,
 585 all other modified residues are localized on coiled regions that face the central binding site of
 586 FadB. This trimethylation, together with the other modifications, are likely important for the
 587 mechanism of action of FadB. In the case of FadD, the residue K493 can interact with the
 588 residue Q526 (A0A1E3M8R8 - UniProt). Trimethylation could change the steric hindrance and
 589 therefore cancel these interactions and the maintenance of the structure.



590
 591 **Figure 5: K-trimethylated proteins were distributed across the whole range of biological**
 592 **functions.** This graph displays proteins involved in DNA metabolism (shades of green), protein
 593 synthesis (shades of blue), protein folding (shades of yellow), drug efflux pumps or porins
 594 (shades of purple) and lipid metabolism (shades of gray). The different PTMs are also

595 represented, with trimethylation (in blue), acetylation (in red) and phosphorylation (in green).
596 For multimeric proteins, the observed PTMs were only shown on a single monomer (e.g.
597 GroEL, GroES). Created with BioRender.com.

598

599 **Multi-modified proteins reveal putative inter-PTMs cross-talks**

600 In a previous study, we characterized N α - and N ϵ -acetylations in *A. baumannii* strain ATCC
601 17978 in planktonic mode of growth¹⁸. Among the trimethylated proteins, eight were acetylated
602 on their N-terminus, such as Tig (A1S_0475), HupB (A1S_1637), GlcB (A1S_1601) and EF-
603 Ts (A1S_2322). Thirty-eight of the trimethylated proteins were previously observed acetylated
604 on lysine residues (Table S2). Of these, six have the same modified K residue (Table S2),
605 including ArgB (A1S_0888), Efp (A1S_2419), FadB (ABYAL0331) and Kbp (A1S_0820).

606 Phosphorylation on serine, threonine and tyrosine has been previously studied in *A. baumannii*
607 ATCC 17978¹⁶ or other strains⁷⁹. Among our trimethylated proteins, 20 have been described
608 to be phosphorylated, such as SucA (A1S_2715), SucB (A1S_2716), HupB, RplK, EF-Ts, or
609 FadB (Table S2). Surprisingly, all of them were also described as acetylated, with the exception
610 of the ribonucleoside-diphosphate reductase (A1S_0746), ObgE (A1S_2498), GroS
611 (A1S_2665), RplK and an unknown protein (A1S_2543).

612 Many of these proteins were discussed above. Here, we can focus on the potassium binding
613 protein Kbp. It was found trimethylated, acetylated and phosphorylated and it was proposed to
614 be a sensor of cytoplasmic potassium enabling adaptation to these environments. The
615 importance of K⁺ uptake has been shown previously and when this mechanism is impaired, it
616 results in a growth defect for *A. baumannii*¹⁰¹. Here, Kbp was detected with three trimethylated
617 lysines (K13, K38, and K138). In our previous study, K138 was also observed acetylated. This
618 residue is localized within the LysM domain and is required to stabilize the BON domain, where
619 potassium binding occurs and then cause conformational change of the BON domain¹⁰². This
620 modified site could impact either the stabilization of these different domains or the
621 conformational changes due to K⁺ binding.

622 The observation of different chemical groups on the same lysine as well as phosphorylation on
623 serine, threonine or tyrosine reveals the presence of several proteoforms for the same protein.
624 PTMs can modulate protein-protein or DNA-protein interactions, change the 3D structure and
625 thus regulate the function of a protein. We recently showed that 3 lysines on major virulence
626 factors in *P. aeruginosa* can be modified by at least 9 different chemical groups. This highlights
627 the need for further investigation of PTMs diversity and cross-talks in *A. baumannii* and notably
628 their modulation of virulence and resistance¹³.

630 CONCLUSION

631 We performed the first large-scale proteomic study of lysine trimethylation in *A. baumannii*
632 strain ATCC 17978 in planktonic and pellicle modes. SCX appears to be the approach of choice
633 to characterize this PTM since in our hands the antibody capture performed poorly. However,
634 this characterization was a fastidious task as sample prefractionation by SCX generates a large
635 number of fractions and therefore a significant time-consuming nLC-MS/MS analysis and data
636 processing. Due to the lack of adequate enrichment strategy, the K-trimethylated peptides were
637 found in sub-stoichiometric quantities making their identification difficult or generally
638 unreliable. This was best highlighted by the poor overlap in identification when comparing the
639 processing results obtained by different database search engines (i.e. Proteome Discoverer,
640 MaxQuant, MetaMorpheus, FragPipe). To focus on the high confidence identifications, we then
641 implemented stringent quality filtering and manually validated all MS/MS spectra of K-
642 trimethylated peptides.

643 Using such a workflow, we were able to identify 84 K-trimethylated proteins. More
644 trimethylated proteins were observed in pellicle modes of growth, although it was not possible
645 to associate specific trimethylation events with distinct growth modes. A large proportion of K-
646 trimethylated proteins were involved in DNA and protein synthesis, membrane biogenesis,
647 transporters or lipid metabolism processes. Trimethylation could thus be an important
648 modification in bacteria to regulate the action of the proteins involved within these functions.
649 By comparing with previous proteomic studies on lysine acetylation, protein N-terminal
650 acetylation and phosphorylation of serine, threonine and tyrosine, we showed the diversity of
651 PTMs used by *A. baumannii*. Several identical lysine residues were observed acetylated or
652 trimethylated, indicating the presence of proteoforms and a potential role of these PTMs in
653 DNA/protein or protein/protein interaction, as suggested by the analysis of some 3D structures.
654 In terms of future work, we envision several avenues of research to improve the identification
655 and characterize the function of trimethylated sites. Notably, here we used CID fragmentation
656 but HCD fragmentation could improve identifications of trimethylated peptides via the presence
657 of diagnostic ions (m/z 130.09)¹⁰³. To investigate the functional role of the trimethylation
658 events, one characterization strategy developed to investigate the histone-code could be
659 applicable to other proteins¹⁰⁴. This approach allows mimicry of trimethylated lysine. This is
660 achieved via mutagenesis into cysteine followed by their alkylation with addition of (2-
661 bromoethyl)-trimethyl-ammonium bromide¹⁰⁵.

662

663 **ACKNOWLEDGMENTS**

664 T.K. thanks the Région Haute-Normandie and the IRIB institute for the PhD financial support.
665 Co-supported by the European Union and Région Normandie. Europe gets involved in
666 Normandie with the European Regional Development Fund (ERDF). This project has received
667 funding from the European Union's Horizon 2020 research and innovation programme under
668 the Marie Skłodowska-Curie grant agreement No 101034329. This project has received funding
669 from the Normandy Region under the WINNINGNormandy program.

670

671 **AUTHOR CONTRIBUTIONS**

672 T.K. and J.H. performed experiments; E.D. and J.H. designed experiments; T.K., N.N. and J.H.
673 analyzed the data; N.N., E.D. and J.H. wrote the paper.

674

675 **SUPPLEMENTARY INFORMATION**

676 Table S1: K-trimethylated sites identified in this study (XLSX).

677 Table S2: Proteins K-trimethylated identified in this study (XLSX).

678 Figure S1: Combination of multiple search engines and filtering criteria to identify K-
679 trimethylated peptides (PDF).

680 Figure S2: The localization of K-trimethylated residues within protein secondary structures
681 (PDF).

682 Figure S3: The abundance of K-trimethylated proteins in different modes of growth (PDF).

683 Figure S4: The repartition of K-trimethylated proteins in terms of functional categories (PDF).

684 Figure S5: Localization of post-translational modifications within protein three-dimensional
685 structure (PDF).

686

687

688

689 REFERENCES

- 690 (1) Boucher, H. W.; Talbot, G. H.; Bradley, J. S.; Edwards, J. E.; Gilbert, D.; Rice, L. B.;
691 Scheld, M.; Spellberg, B.; Bartlett, J. Bad bugs, no drugs: no ESKAPE! An update from the
692 Infectious Diseases Society of America. *Clin Infect Dis* **2009**, *48* (1), 1-12. DOI:
693 10.1086/595011.
- 694 (2) Peleg, A. Y.; Seifert, H.; Paterson, D. L. Acinetobacter baumannii: emergence of a
695 successful pathogen. *Clin Microbiol Rev* **2008**, *21* (3), 538-582. DOI: 10.1128/CMR.00058-07.
- 696 (3) Di Venanzio, G.; Flores-Mireles, A. L.; Calix, J. J.; Haurat, M. F.; Scott, N. E.; Palmer, L.
697 D.; Potter, R. F.; Hibbing, M. E.; Friedman, L.; Wang, B.; et al. Urinary tract colonization is
698 enhanced by a plasmid that regulates uropathogenic Acinetobacter baumannii chromosomal
699 genes. *Nat Commun* **2019**, *10* (1), 2763. DOI: 10.1038/s41467-019-10706-y From NLM.
- 700 (4) Dijkshoorn, L.; Nemec, A.; Seifert, H. An increasing threat in hospitals: multidrug-resistant
701 Acinetobacter baumannii. *Nat Rev Microbiol* **2007**, *5* (12), 939-951. DOI:
702 10.1038/nrmicro1789.
- 703 (5) Sengstock, D. M.; Thyagarajan, R.; Apalara, J.; Mira, A.; Chopra, T.; Kaye, K. S.
704 Multidrug-resistant Acinetobacter baumannii: an emerging pathogen among older adults in
705 community hospitals and nursing homes. *Clin Infect Dis* **2010**, *50* (12), 1611-1616. DOI:
706 10.1086/652759.
- 707 (6) Gayoso, C. M.; Mateos, J.; Mendez, J. A.; Fernandez-Puente, P.; Rumbo, C.; Tomas, M.;
708 Martinez de Ilarduya, O.; Bou, G. Molecular mechanisms involved in the response to
709 desiccation stress and persistence in Acinetobacter baumannii. *J Proteome Res* **2014**, *13* (2),
710 460-476. DOI: 10.1021/pr400603f.
- 711 (7) Soares, N. C.; Cabral, M. P.; Gayoso, C.; Mallo, S.; Rodriguez-Velo, P.; Fernandez-Moreira,
712 E.; Bou, G. Associating growth-phase-related changes in the proteome of Acinetobacter
713 baumannii with increased resistance to oxidative stress. *J Proteome Res* **2010**, *9* (4), 1951-1964.
714 DOI: 10.1021/pr901116r.
- 715 (8) Rodriguez-Bano, J.; Marti, S.; Soto, S.; Fernandez-Cuenca, F.; Cisneros, J. M.; Pachon, J.;
716 Pascual, A.; Martinez-Martinez, L.; McQueary, C.; Actis, L. A.; et al. Biofilm formation in
717 Acinetobacter baumannii: associated features and clinical implications. *Clin Microbiol Infect*
718 **2008**, *14* (3), 276-278. DOI: 10.1111/j.1469-0691.2007.01916.x.
- 719 (9) Zeighami, H.; Valadkhani, F.; Shapouri, R.; Samadi, E.; Haghi, F. Virulence characteristics
720 of multidrug resistant biofilm forming Acinetobacter baumannii isolated from intensive care
721 unit patients. *BMC Infectious Diseases* **2019**, *19* (1), 629. DOI: 10.1186/s12879-019-4272-0.
- 722 (10) Greene, C.; Vadlamudi, G.; Newton, D.; Foxman, B.; Xi, C. The influence of biofilm
723 formation and multidrug resistance on environmental survival of clinical and environmental
724 isolates of Acinetobacter baumannii. *Am J Infect Control* **2016**, *44* (5), e65-71. DOI:
725 10.1016/j.ajic.2015.12.012.
- 726 (11) Lee, H. W.; Koh, Y. M.; Kim, J.; Lee, J. C.; Lee, Y. C.; Seol, S. Y.; Cho, D. T.; Kim, J.
727 Capacity of multidrug-resistant clinical isolates of Acinetobacter baumannii to form biofilm
728 and adhere to epithelial cell surfaces. *Clin Microbiol Infect* **2008**, *14* (1), 49-54. DOI:
729 10.1111/j.1469-0691.2007.01842.x.
- 730 (12) Marti, S.; Rodriguez-Bano, J.; Catel-Ferreira, M.; Jouenne, T.; Vila, J.; Seifert, H.; De, E.
731 Biofilm formation at the solid-liquid and air-liquid interfaces by Acinetobacter species. *BMC*
732 *Res Notes* **2011**, *4*, 5. DOI: 10.1186/1756-0500-4-5.
- 733 (13) Macek, B.; Forchhammer, K.; Hardouin, J.; Weber-Ban, E.; Grangeasse, C.; Mijakovic, I.
734 Protein post-translational modifications in bacteria. *Nat Rev Microbiol* **2019**, *17* (11), 651-664.
735 DOI: 10.1038/s41579-019-0243-0.
- 736 (14) Iwashkiw, J. A.; Seper, A.; Weber, B. S.; Scott, N. E.; Vinogradov, E.; Stratilo, C.; Reiz,
737 B.; Cordwell, S. J.; Whittal, R.; Schild, S.; et al. Identification of a general O-linked protein

738 glycosylation system in *Acinetobacter baumannii* and its role in virulence and biofilm
739 formation. *PLoS Pathog* **2012**, *8* (6), e1002758. DOI: 10.1371/journal.ppat.1002758.

740 (15) Lai, J. H.; Yang, J. T.; Chern, J.; Chen, T. L.; Wu, W. L.; Liao, J. H.; Tsai, S. F.; Liang, S.
741 Y.; Chou, C. C.; Wu, S. H. Comparative Phosphoproteomics Reveals the Role of AmpC beta-
742 lactamase Phosphorylation in the Clinical Imipenem-resistant Strain *Acinetobacter baumannii*
743 SK17. *Mol Cell Proteomics* **2016**, *15* (1), 12-25. DOI: 10.1074/mcp.M115.051052.

744 (16) Soares, N. C.; Spat, P.; Mendez, J. A.; Nakedi, K.; Aranda, J.; Bou, G. Ser/Thr/Tyr
745 phosphoproteome characterization of *Acinetobacter baumannii*: comparison between a
746 reference strain and a highly invasive multidrug-resistant clinical isolate. *J Proteomics* **2014**,
747 *102*, 113-124. DOI: 10.1016/j.jprot.2014.03.009.

748 (17) Massier, S.; Robin, B.; Megroz, M.; Wright, A.; Harper, M.; Hayes, B.; Cosette, P.;
749 Broutin, I.; Boyce, J. D.; De, E.; et al. Phosphorylation of Extracellular Proteins in
750 *Acinetobacter baumannii* in Sessile Mode of Growth. *Front Microbiol* **2021**, *12*, 738780. DOI:
751 10.3389/fmicb.2021.738780.

752 (18) Kentache, T.; Jouenne, T.; De, E.; Hardouin, J. Proteomic characterization of Nalpha- and
753 Nepsilon-acetylation in *Acinetobacter baumannii*. *J Proteomics* **2016**, *144*, 148-158. DOI:
754 10.1016/j.jprot.2016.05.021.

755 (19) Alban, C.; Tardif, M.; Mininno, M.; Brugiére, S.; Gilgen, A.; Ma, S.; Mazzoleni, M.;
756 Gigarel, O.; Martin-Laffon, J.; Ferro, M.; et al. Uncovering the protein lysine and arginine
757 methylation network in *Arabidopsis chloroplasts*. *PLoS One* **2014**, *9* (4), e95512. DOI:
758 10.1371/journal.pone.0095512.

759 (20) Lanouette, S.; Davey, J. A.; Elisma, F.; Ning, Z.; Figeys, D.; Chica, R. A.; Couture, J. F.
760 Discovery of substrates for a SET domain lysine methyltransferase predicted by multistate
761 computational protein design. *Structure* **2015**, *23* (1), 206-215. DOI: 10.1016/j.str.2014.11.004.

762 (21) Maas, M. N.; Hintzen, J. C. J.; Porzberg, M. R. B.; Mecinovic, J. Trimethyllysine: From
763 Carnitine Biosynthesis to Epigenetics. *Int J Mol Sci* **2020**, *21* (24). DOI:
764 10.3390/ijms21249451.

765 (22) Fraga, M. F.; Ballestar, E.; Villar-Garea, A.; Boix-Chornet, M.; Espada, J.; Schotta, G.;
766 Bonaldi, T.; Haydon, C.; Ropero, S.; Petrie, K.; et al. Loss of acetylation at Lys16 and
767 trimethylation at Lys20 of histone H4 is a common hallmark of human cancer. *Nature Genetics*
768 **2005**, *37* (4), 391-400. DOI: 10.1038/ng1531.

769 (23) Schmidt, A.; Kochanowski, K.; Vedelaar, S.; Ahrne, E.; Volkmer, B.; Callipo, L.; Knoop,
770 K.; Bauer, M.; Aebersold, R.; Heinemann, M. The quantitative and condition-dependent
771 *Escherichia coli* proteome. *Nat Biotechnol* **2016**, *34* (1), 104-110. DOI: 10.1038/nbt.3418.

772 (24) Abeykoon, A. H.; Chao, C. C.; Wang, G.; Gucek, M.; Yang, D. C.; Ching, W. M. Two
773 protein lysine methyltransferases methylate outer membrane protein B from *Rickettsia*. *J*
774 *Bacteriol* **2012**, *194* (23), 6410-6418. DOI: 10.1128/JB.01379-12.

775 (25) Turco, J.; Winkler, H. H. Cytokine sensitivity and methylation of lysine in *Rickettsia*
776 *proWazekii* EVir and interferon-resistant *R. prowazekii* strains. *Infect Immun* **1994**, *62* (8),
777 3172-3177. DOI: 10.1128/iai.62.8.3172-3177.1994.

778 (26) Marti, S.; Nait Chabane, Y.; Alexandre, S.; Coquet, L.; Vila, J.; Jouenne, T.; De, E. Growth
779 of *Acinetobacter baumannii* in pellicle enhanced the expression of potential virulence factors.
780 *PLoS One* **2011**, *6* (10), e26030. DOI: 10.1371/journal.pone.0026030.

781 (27) Ouidir, T.; Cosette, P.; Jouenne, T.; Hardouin, J. Proteomic profiling of lysine acetylation
782 in *Pseudomonas aeruginosa* reveals the diversity of acetylated proteins. *Proteomics* **2015**, *15*
783 (13), 2152-2157. DOI: 10.1002/pmic.201500056.

784 (28) Vizcaino, J. A.; Deutsch, E. W.; Wang, R.; Csordas, A.; Reisinger, F.; Rios, D.; Dianes, J.
785 A.; Sun, Z.; Farrah, T.; Bandeira, N.; et al. ProteomeXchange provides globally coordinated
786 proteomics data submission and dissemination. *Nat Biotechnol* **2014**, *32* (3), 223-226. DOI:
787 10.1038/nbt.2839.

788 (29) Orsburn, B. C. Proteome Discoverer-A Community Enhanced Data Processing Suite for
789 Protein Informatics. *Proteomes* **2021**, 9 (1). DOI: 10.3390/proteomes9010015 From NLM.

790 (30) Cox, J.; Mann, M. MaxQuant enables high peptide identification rates, individualized
791 p.p.b.-range mass accuracies and proteome-wide protein quantification. *Nat Biotechnol* **2008**,
792 26 (12), 1367-1372. DOI: 10.1038/nbt.1511.

793 (31) Yu, F.; Teo, G. C.; Kong, A. T.; Haynes, S. E.; Avtonomov, D. M.; Geiszler, D. J.;
794 Nesvizhskii, A. I. Identification of modified peptides using localization-aware open search.
795 *Nature Communications* **2020**, 11 (1), 4065. DOI: 10.1038/s41467-020-17921-y.

796 (32) Solntsev, S. K.; Shortreed, M. R.; Frey, B. L.; Smith, L. M. Enhanced Global Post-
797 translational Modification Discovery with MetaMorpheus. *Journal of Proteome Research*
798 **2018**, 17 (5), 1844-1851. DOI: 10.1021/acs.jproteome.7b00873.

799 (33) Vallenet, D.; Belda, E.; Calteau, A.; Cruveiller, S.; Engelen, S.; Lajus, A.; Le Fevre, F.;
800 Longin, C.; Mornico, D.; Roche, D.; et al. MicroScope--an integrated microbial resource for
801 the curation and comparative analysis of genomic and metabolic data. *Nucleic Acids Res* **2013**,
802 41 (Database issue), D636-647. DOI: 10.1093/nar/gks1194.

803 (34) Tatusov, R. L.; Koonin, E. V.; Lipman, D. J. A genomic perspective on protein families.
804 *Science* **1997**, 278 (5338), 631-637.

805 (35) Blum, M.; Chang, H.-Y.; Chuguransky, S.; Grego, T.; Kandasamy, S.; Mitchell, A.; Nuka,
806 G.; Paysan-Lafosse, T.; Qureshi, M.; Raj, S.; et al. The InterPro protein families and domains
807 database: 20 years on. *Nucleic Acids Research* **2021**, 49 (D1), D344-D354. DOI:
808 10.1093/nar/gkaa977 (accessed 2/4/2021).

809 (36) Huerta-Cepas, J.; Forslund, K.; Coelho, L. P.; Szklarczyk, D.; Jensen, L. J.; von Mering,
810 C.; Bork, P. Fast Genome-Wide Functional Annotation through Orthology Assignment by
811 eggNOG-Mapper. *Molecular Biology and Evolution* **2017**, 34 (8), 2115-2122. DOI:
812 10.1093/molbev/msx148.

813 (37) Tatusov, R. L.; Galperin, M. Y.; Natale, D. A.; Koonin, E. V. The COG database: a tool
814 for genome-scale analysis of protein functions and evolution. *Nucleic Acids Res* **2000**, 28 (1),
815 33-36.

816 (38) Høie, M. H.; Kiehl, E. N.; Petersen, B.; Nielsen, M.; Winther, O.; Nielsen, H.; Hallgren,
817 J.; Marcatili, P. NetSurfP-3.0: accurate and fast prediction of protein structural features by
818 protein language models and deep learning. *Nucleic Acids Research* **2022**, 50 (W1), W510-
819 W515. DOI: 10.1093/nar/gkac439 (accessed 12/28/2022).

820 (39) Wagih, O.; Sugiyama, N.; Ishihama, Y.; Beltrao, P. Uncovering Phosphorylation-Based
821 Specificities through Functional Interaction Networks. *Mol Cell Proteomics* **2016**, 15 (1), 236-
822 245. DOI: 10.1074/mcp.M115.052357 From NLM.

823 (40) Yu, G.; Wang, L. G.; Han, Y.; He, Q. Y. clusterProfiler: an R package for comparing
824 biological themes among gene clusters. *OMICS* **2012**, 16 (5), 284-287. DOI:
825 10.1089/omi.2011.0118.

826 (41) Jumper, J.; Evans, R.; Pritzel, A.; Green, T.; Figurnov, M.; Ronneberger, O.;
827 Tunyasuvunakool, K.; Bates, R.; Židek, A.; Potapenko, A.; et al. Highly accurate protein
828 structure prediction with AlphaFold. *Nature* **2021**, 596 (7873), 583-589. DOI: 10.1038/s41586-
829 021-03819-2.

830 (42) Burley, S. K.; Bhikadiya, C.; Bi, C.; Bittrich, S.; Chao, H.; Chen, L.; Craig, P. A.;
831 Crichlow, G. V.; Dalenberg, K.; Duarte, J. M.; et al. RCSB Protein Data Bank (RCSB.org):
832 delivery of experimentally-determined PDB structures alongside one million computed
833 structure models of proteins from artificial intelligence/machine learning. *Nucleic Acids*
834 *Research* **2023**, 51 (D1), D488-D508. DOI: 10.1093/nar/gkac1077 (accessed 1/16/2023).

835 (43) Camacho, C.; Coulouris, G.; Avagyan, V.; Ma, N.; Papadopoulos, J.; Bealer, K.; Madden,
836 T. L. BLAST+: architecture and applications. *BMC Bioinformatics* **2009**, 10, 421. DOI:
837 10.1186/1471-2105-10-421.

838 (44) Cao, X.-J.; Arnaudo, A. M.; Garcia, B. A. Large-scale global identification of protein
839 lysine methylation in vivo. *Epigenetics* **2013**, *8* (5), 477-485. DOI: 10.4161/epi.24547.

840 (45) Kaur, I.; Zeeshan, M.; Saini, E.; Kaushik, A.; Mohmmed, A.; Gupta, D.; Malhotra, P.
841 Widespread occurrence of lysine methylation in Plasmodium falciparum proteins at asexual
842 blood stages. *Scientific Reports* **2016**, *6* (1), 35432. DOI: 10.1038/srep35432.

843 (46) Iakoucheva, L. M.; Radivojac, P.; Brown, C. J.; O'Connor, T. R.; Sikes, J. G.; Obradovic,
844 Z.; Dunker, A. K. The importance of intrinsic disorder for protein phosphorylation. *Nucleic
845 Acids Research* **2004**, *32* (3), 1037-1049. DOI: 10.1093/nar/gkh253 (accessed 11/30/2022).

846 (47) Kamacioglu, A.; Tuncbag, N.; Ozlu, N. Structural analysis of mammalian protein
847 phosphorylation at a proteome level. *Structure* **2021**, *29* (11), 1219-1229.e1213. DOI:
848 <https://doi.org/10.1016/j.str.2021.06.008>.

849 (48) Kuiper, E. G.; Dey, D.; LaMore, P. A.; Owings, J. P.; Prezioso, S. M.; Goldberg, J. B.;
850 Conn, G. L. Substrate recognition by the Pseudomonas aeruginosa EF-Tu-modifying
851 methyltransferase EftM. *J Biol Chem* **2019**, *294* (52), 20109-20121. DOI:
852 10.1074/jbc.RA119.011213 From NLM.

853 (49) Wang, C.; Nehls, C.; Baabe, D.; Burghaus, O.; Hurwitz, R.; Gutschmann, T.; Bröring, M.;
854 Kolbe, M. Flagellin lysine methyltransferase FliB catalyzes a [4Fe-4S] mediated methyl
855 transfer reaction. *PLOS Pathogens* **2021**, *17* (11), e1010052. DOI:
856 10.1371/journal.ppat.1010052.

857 (50) Kentache, T.; Ben Abdelkrim, A.; Jouenne, T.; De, E.; Hardouin, J. Global Dynamic
858 Proteome Study of a Pellicle-forming Acinetobacter baumannii Strain. *Mol Cell Proteomics*
859 **2017**, *16* (1), 100-112. DOI: 10.1074/mcp.M116.061044.

860 (51) Chen, W.-H.; Minguez, P.; Lercher, M. J.; Bork, P. OGEE: an online gene essentiality
861 database. *Nucleic Acids Research* **2011**, *40* (D1), D901-D906. DOI: 10.1093/nar/gkr986
862 (accessed 11/24/2022).

863 (52) Carabetta, V. J. Addressing the Possibility of a Histone-Like Code in Bacteria. *J Proteome
864 Res* **2021**, *20* (1), 27-37. DOI: 10.1021/acs.jproteome.0c00442.

865 (53) Xu, J. Y.; Xu, Z.; Liu, X.; Tan, M.; Ye, B. C. Protein Acetylation and Butyrylation Regulate
866 the Phenotype and Metabolic Shifts of the Endospore-forming Clostridium acetobutylicum.
867 *Mol Cell Proteomics* **2018**, *17* (6), 1156-1169. DOI: 10.1074/mcp.RA117.000372.

868 (54) Chen, J.; Xie, J. Role and regulation of bacterial LuxR-like regulators. *Journal of Cellular
869 Biochemistry* **2011**, *112* (10), 2694-2702, <https://doi.org/10.1002/jcb.23219>. DOI:
870 <https://doi.org/10.1002/jcb.23219> (accessed 2023/01/17).

871 (55) Oh, M. H.; Choi, C. H. Role of LuxIR Homologue AnoIR in Acinetobacter nosocomialis
872 and the Effect of Virstatin on the Expression of anoR Gene. *J Microbiol Biotechnol* **2015**, *25*
873 (8), 1390-1400. DOI: 10.4014/jmb.1504.04069.

874 (56) Bae, B.; Feklistov, A.; Lass-Napiorkowska, A.; Landick, R.; Darst, S. A. Structure of a
875 bacterial RNA polymerase holoenzyme open promoter complex. *eLife* **2015**, *4*, e08504. DOI:
876 10.7554/eLife.08504.

877 (57) Lee, Y. H.; Nam, K. H.; Helmann, J. D. A mutation of the RNA polymerase β' subunit
878 (rpoC) confers cephalosporin resistance in Bacillus subtilis. *Antimicrob Agents Chemother*
879 **2013**, *57* (1), 56-65. DOI: 10.1128/aac.01449-12 From NLM.

880 (58) Bouakaz, L.; Bouakaz, E.; Murgola, E. J.; Ehrenberg, M.; Sanyal, S. The Role of
881 Ribosomal Protein L11 in Class I Release Factor-mediated Translation Termination and
882 Translational Accuracy*. *Journal of Biological Chemistry* **2006**, *281* (7), 4548-4556. DOI:
883 <https://doi.org/10.1074/jbc.M510433200>.

884 (59) Dognin, M. J.; Wittmann-Liebold, B. Purification and primary structure determination of
885 the N-terminal blocked protein, L11, from Escherichia coli ribosomes. *Eur J Biochem* **1980**,
886 *112* (1), 131-151. DOI: 10.1111/j.1432-1033.1980.tb04995.x.

887 (60) Lederer, F.; Alix, J. H.; Hayes, D. N-Trimethylalanine, a novel blocking group, found in
888 E. coli ribosomal protein L11. *Biochem Biophys Res Commun* **1977**, *77* (2), 470-480. DOI:
889 10.1016/s0006-291x(77)80004-1.

890 (61) Cameron, D. M.; Gregory, S. T.; Thompson, J.; Suh, M. J.; Limbach, P. A.; Dahlberg, A.
891 E. *Thermus thermophilus* L11 methyltransferase, PrmA, is dispensable for growth and
892 preferentially modifies free ribosomal protein L11 prior to ribosome assembly. *J Bacteriol*
893 **2004**, *186* (17), 5819-5825. DOI: 10.1128/JB.186.17.5819-5825.2004.

894 (62) Agrawal, R. K.; Linde, J.; Sengupta, J.; Nierhaus, K. H.; Frank, J. Localization of L11
895 protein on the ribosome and elucidation of its involvement in EF-G-dependent translocation. *J*
896 *Mol Biol* **2001**, *311* (4), 777-787. DOI: 10.1006/jmbi.2001.4907 From NLM.

897 (63) Yang, X.; Ishiguro Edward, E. Involvement of the N Terminus of Ribosomal Protein L11
898 in Regulation of the RelA Protein of Escherichia coli. *Journal of Bacteriology* **2001**, *183* (22),
899 6532-6537. DOI: 10.1128/JB.183.22.6532-6537.2001 (accessed 2023/01/17).

900 (64) Roy, S.; Chowdhury, G.; Mukhopadhyay, A. K.; Dutta, S.; Basu, S. Convergence of
901 Biofilm Formation and Antibiotic Resistance in *Acinetobacter baumannii* Infection. *Front Med*
902 *(Lausanne)* **2022**, *9*, 793615. DOI: 10.3389/fmed.2022.793615 From NLM.

903 (65) Ranieri Michael, R. M.; Chan Derek, C. K.; Yaeger Luke, N.; Rudolph, M.; Karabelas-
904 Pittman, S.; Abdo, H.; Chee, J.; Harvey, H.; Nguyen, U.; Burrows Lori, L. Thiostrepton Hijacks
905 Pyoverdine Receptors To Inhibit Growth of *Pseudomonas aeruginosa*. *Antimicrobial Agents*
906 *and Chemotherapy* **2019**, *63* (9), e00472-00419. DOI: 10.1128/AAC.00472-19 (accessed
907 2022/12/01).

908 (66) Boël, G.; Smith, P. C.; Ning, W.; Englander, M. T.; Chen, B.; Hashem, Y.; Testa, A. J.;
909 Fischer, J. J.; Wieden, H. J.; Frank, J.; et al. The ABC-F protein EttA gates ribosome entry into
910 the translation elongation cycle. *Nat Struct Mol Biol* **2014**, *21* (2), 143-151. DOI:
911 10.1038/nsmb.2740 From NLM.

912 (67) Ben-Chetrit, N.; Niu, X.; Swett, A. D.; Sotelo, J.; Jiao, M. S.; Stewart, C. M.; Potenski, C.;
913 Mielinis, P.; Roelli, P.; Stoeckius, M.; et al. Integration of whole transcriptome spatial profiling
914 with protein markers. *Nature Biotechnology* **2023**. DOI: 10.1038/s41587-022-01536-3.

915 (68) Kawashima, T.; Berthet-Colominas, C.; Wulff, M.; Cusack, S.; Leberman, R. The structure
916 of the Escherichia coli EF-Tu·EF-Ts complex at 2.5 Å resolution. *Nature* **1996**, *379* (6565),
917 511-518. DOI: 10.1038/379511a0.

918 (69) Burnett, B. J.; Altman, R. B.; Ferrao, R.; Alejo, J. L.; Kaur, N.; Kanji, J.; Blanchard, S. C.
919 Elongation factor Ts directly facilitates the formation and disassembly of the Escherichia coli
920 elongation factor Tu·GTP·aminoacyl-tRNA ternary complex. *J Biol Chem* **2013**, *288* (19),
921 13917-13928. DOI: 10.1074/jbc.M113.460014 From NLM.

922 (70) Su, V.; Lau, A. F. Ubiquitin-like and ubiquitin-associated domain proteins: significance in
923 proteasomal degradation. *Cell Mol Life Sci* **2009**, *66* (17), 2819-2833. DOI: 10.1007/s00018-
924 009-0048-9 From NLM.

925 (71) Qin, Y.; Polacek, N.; Vesper, O.; Staub, E.; Einfeldt, E.; Wilson, D. N.; Nierhaus, K. H.
926 The Highly Conserved LepA Is a Ribosomal Elongation Factor that Back-Translocates the
927 Ribosome. *Cell* **2006**, *127* (4), 721-733. DOI: 10.1016/j.cell.2006.09.037 (accessed
928 2023/01/09).

929 (72) Chiappori, F.; Fumian, M.; Milanese, L.; Merelli, I. DnaK as Antibiotic Target: Hot Spot
930 Residues Analysis for Differential Inhibition of the Bacterial Protein in Comparison with the
931 Human HSP70. *PLOS ONE* **2015**, *10* (4), e0124563. DOI: 10.1371/journal.pone.0124563.

932 (73) Knappe, D.; Zahn, M.; Sauer, U.; Schiffer, G.; Sträter, N.; Hoffmann, R. Rational Design
933 of Oncocin Derivatives with Superior Protease Stabilities and Antibacterial Activities Based on
934 the High-Resolution Structure of the Oncocin-DnaK Complex. *ChemBioChem* **2011**, *12* (6),
935 874-876, <https://doi.org/10.1002/cbic.201000792>. DOI:
936 <https://doi.org/10.1002/cbic.201000792> (accessed 2023/01/17).

937 (74) Liu, Y.; Gierasch, L. M.; Bahar, I. Role of Hsp70 ATPase Domain Intrinsic Dynamics and
938 Sequence Evolution in Enabling its Functional Interactions with NEFs. *PLOS Computational*
939 *Biology* **2010**, *6* (9), e1000931. DOI: 10.1371/journal.pcbi.1000931.

940 (75) Balchin, D.; Hayer-Hartl, M.; Hartl, F. U. In vivo aspects of protein folding and quality
941 control. *Science* **2016**, *353* (6294), aac4354. DOI: 10.1126/science.aac4354 (accessed
942 2023/01/18).

943 (76) Jaworek, M. W.; Mobitz, S.; Gao, M.; Winter, R. Stability of the chaperonin system
944 GroEL-GroES under extreme environmental conditions. *Phys Chem Chem Phys* **2020**, *22* (6),
945 3734-3743. DOI: 10.1039/c9cp06468k.

946 (77) Goltermann, L.; Sarusie, M. V.; Bentin, T. Chaperonin GroEL/GroES Over-Expression
947 Promotes Aminoglycoside Resistance and Reduces Drug Susceptibilities in Escherichia coli
948 Following Exposure to Sublethal Aminoglycoside Doses. *Front Microbiol* **2015**, *6*, 1572. DOI:
949 10.3389/fmicb.2015.01572 From NLM.

950 (78) Cardoso, K.; Gandra, R. F.; Wisniewski, E. S.; Osaku, C. A.; Kadowaki, M. K.; Felipach-
951 Neto, V.; Haus, L. F. A.-Á.; Simão, R. d. C. G. DnaK and GroEL are induced in response to
952 antibiotic and heat shock in Acinetobacter baumannii. *Journal of Medical Microbiology* **2010**,
953 *59* (9), 1061-1068. DOI: <https://doi.org/10.1099/jmm.0.020339-0>.

954 (79) Li, Z.; Li, S.; Luo, M.; Jhong, J.-H.; Li, W.; Yao, L.; Pang, Y.; Wang, Z.; Wang, R.; Ma,
955 R.; et al. dbPTM in 2022: an updated database for exploring regulatory networks and functional
956 associations of protein post-translational modifications. *Nucleic Acids Research* **2021**, *50* (D1),
957 D471-D479. DOI: 10.1093/nar/gkab1017 (accessed 2/8/2022).

958 (80) Li, Z.; Wang, Y.; Yao, Q.; Justice, N. B.; Ahn, T.-H.; Xu, D.; Hettich, R. L.; Banfield, J.
959 F.; Pan, C. Diverse and divergent protein post-translational modifications in two growth stages
960 of a natural microbial community. *Nature Communications* **2014**, *5* (1), 4405. DOI:
961 10.1038/ncomms5405.

962 (81) Faoro, C.; Wilkinson-White, L.; Kwan, A. H.; Ataide, S. F. Discovery of fragments that
963 target key interactions in the signal recognition particle (SRP) as potential leads for a new class
964 of antibiotics. *PLOS ONE* **2018**, *13* (7), e0200387. DOI: 10.1371/journal.pone.0200387.

965 (82) Draycheva, A.; Bornemann, T.; Ryazanov, S.; Lakomek, N.-A.; Wintermeyer, W. The
966 bacterial SRP receptor, FtsY, is activated on binding to the translocon. *Molecular Microbiology*
967 **2016**, *102* (1), 152-167, <https://doi.org/10.1111/mmi.13452>. DOI:
968 <https://doi.org/10.1111/mmi.13452> (accessed 2023/01/09).

969 (83) Vila, J.; Marti, S.; Sanchez-Cespedes, J. Porins, efflux pumps and multidrug resistance in
970 Acinetobacter baumannii. *J Antimicrob Chemother* **2007**, *59* (6), 1210-1215. DOI:
971 10.1093/jac/dkl509.

972 (84) Bhamidimarri, S. P.; Zahn, M.; Prajapati, J. D.; Schleberger, C.; Söderholm, S.; Hoover,
973 J.; West, J.; Kleinekathöfer, U.; Bumann, D.; Winterhalter, M.; et al. A Multidisciplinary
974 Approach toward Identification of Antibiotic Scaffolds for Acinetobacter
975 baumannii. *Structure* **2019**, *27* (2), 268-280.e266. DOI: 10.1016/j.str.2018.10.021
976 (accessed 2022/12/01).

977 (85) Vashist, J.; Tiwari, V.; Kapil, A.; Rajeswari, M. R. Quantitative Profiling and Identification
978 of Outer Membrane Proteins of β -Lactam Resistant Strain of Acinetobacter baumannii. *Journal*
979 *of Proteome Research* **2010**, *9* (2), 1121-1128. DOI: 10.1021/pr9011188.

980 (86) Fereshteh, S.; Abdoli, S.; Shahcheraghi, F.; Ajdary, S.; Nazari, M.; Badmasti, F. New
981 putative vaccine candidates against Acinetobacter baumannii using the reverse vaccinology
982 method. *Microbial Pathogenesis* **2020**, *143*, 104114. DOI:
983 <https://doi.org/10.1016/j.micpath.2020.104114>.

984 (87) Prajapati, J. D.; Kleinekathöfer, U.; Winterhalter, M. How to Enter a Bacterium: Bacterial
985 Porins and the Permeation of Antibiotics. *Chemical Reviews* **2021**, *121* (9), 5158-5192. DOI:
986 10.1021/acs.chemrev.0c01213.

987 (88) Sheldon, J. R.; Skaar, E. P. *Acinetobacter baumannii* can use multiple siderophores for
988 iron acquisition, but only acinetobactin is required for virulence. *PLoS Pathog* **2020**, *16* (10),
989 e1008995. DOI: 10.1371/journal.ppat.1008995 From NLM.

990 (89) Li, C.; Pan, D.; Li, M.; Wang, Y.; Song, L.; Yu, D.; Zuo, Y.; Wang, K.; Liu, Y.; Wei, Z.;
991 et al. Aerobactin-Mediated Iron Acquisition Enhances Biofilm Formation, Oxidative Stress
992 Resistance, and Virulence of *Yersinia pseudotuberculosis*. *Frontiers in Microbiology* **2021**, *12*,
993 Original Research. DOI: 10.3389/fmicb.2021.699913.

994 (90) Aghajani, Z.; Rasooli, I.; Mousavi Gargari, S. L. Exploitation of two siderophore receptors,
995 BauA and BfnH, for protection against *Acinetobacter baumannii* infection. *APMIS* **2019**, *127*
996 (12), 753-763. DOI: <https://doi.org/10.1111/apm.12992>.

997 (91) Shvarev, D.; Nishi, C. N.; Maldener, I. Two DevBCA-like ABC transporters are involved
998 in the multidrug resistance of the cyanobacterium *Anabaena* sp. PCC 7120. *FEBS Letters* **2019**,
999 *593* (14), 1818-1826, <https://doi.org/10.1002/1873-3468.13450>. DOI:
1000 <https://doi.org/10.1002/1873-3468.13450> (accessed 2022/12/01).

1001 (92) Wang, Z.; Zhong, M.; Lu, W.; Chai, Q.; Wei, Y. Repressive mutations restore function-
1002 loss caused by the disruption of trimerization in *Escherichia coli* multidrug transporter AcrB.
1003 *Frontiers in Microbiology* **2015**, *6*, Original Research. DOI: 10.3389/fmicb.2015.00004.

1004 (93) Yuhan, Y.; Ziyun, Y.; Yongbo, Z.; Fuqiang, L.; Qinghua, Z. Over expression of AdeABC
1005 and AcrAB-TolC efflux systems confers tigecycline resistance in clinical isolates of
1006 *Acinetobacter baumannii* and *Klebsiella pneumoniae*. *Rev Soc Bras Med Trop* **2016**, *49* (2),
1007 165-171. DOI: 10.1590/0037-8682-0411-2015 From NLM.

1008 (94) Subhadra, B.; Surendran, S.; Lim, B. R.; Yim, J. S.; Kim, D. H.; Woo, K.; Kim, H.-J.; Oh,
1009 M. H.; Choi, C. H. Regulation of the AcrAB efflux system by the quorum-sensing regulator
1010 AnoR in *Acinetobacter nosocomialis*. *Journal of Microbiology* **2020**, *58* (6), 507-518. DOI:
1011 10.1007/s12275-020-0185-2.

1012 (95) Tam, H. K.; Foong, W. E.; Oswald, C.; Herrmann, A.; Zeng, H.; Pos, K. M. Allosteric
1013 drug transport mechanism of multidrug transporter AcrB. *Nat Commun* **2021**, *12* (1), 3889.
1014 DOI: 10.1038/s41467-021-24151-3.

1015 (96) Tram, G.; Poole, J.; Adams, F. G.; Jennings, M. P.; Eijkelkamp, B. A.; Atack, J. M. The
1016 *Acinetobacter baumannii* Autotransporter Adhesin Ata Recognizes Host Glycans as High-
1017 Affinity Receptors. *ACS Infectious Diseases* **2021**, *7* (8), 2352-2361. DOI:
1018 10.1021/acsinfecdis.1c00021.

1019 (97) Jiang, J. H.; Hassan, K. A.; Begg, S. L.; Rupasinghe, T. W. T.; Naidu, V.; Pederick, V. G.;
1020 Khorvash, M.; Whittall, J. J.; Paton, J. C.; Paulsen, I. T.; et al. Identification of Novel
1021 *Acinetobacter baumannii* Host Fatty Acid Stress Adaptation Strategies. *mBio* **2019**, *10* (1).
1022 DOI: 10.1128/mBio.02056-18 From NLM.

1023 (98) Blázquez, B.; Carmona, M.; García, J. L.; Díaz, E. Identification and analysis of a glutaryl-
1024 CoA dehydrogenase-encoding gene and its cognate transcriptional regulator from *Azoarcus* sp.
1025 CIB. *Environmental Microbiology* **2008**, *10* (2), 474-482, [https://doi.org/10.1111/j.1462-](https://doi.org/10.1111/j.1462-2920.2007.01468.x)
1026 [2920.2007.01468.x](https://doi.org/10.1111/j.1462-2920.2007.01468.x). DOI: <https://doi.org/10.1111/j.1462-2920.2007.01468.x> (accessed
1027 2023/01/12).

1028 (99) Fujita, Y.; Matsuoka, H.; Hirooka, K. Regulation of fatty acid metabolism in bacteria. *Mol*
1029 *Microbiol* **2007**, *66* (4), 829-839. DOI: 10.1111/j.1365-2958.2007.05947.x.

1030 (100) Hamed, R. B.; Batchelar, E. T.; Clifton, I. J.; Schofield, C. J. Mechanisms and structures
1031 of crotonase superfamily enzymes – How nature controls enolate and oxyanion reactivity.
1032 *Cellular and Molecular Life Sciences* **2008**, *65* (16), 2507-2527. DOI: 10.1007/s00018-008-
1033 8082-6.

1034 (101) König, P.; Averhoff, B.; Müller, V. K⁺ and its role in virulence of *Acinetobacter*
1035 *baumannii*. *International Journal of Medical Microbiology* **2021**, *311* (5), 151516. DOI:
1036 <https://doi.org/10.1016/j.ijmm.2021.151516>.

1037 (102) Ashraf, Khuram U.; Josts, I.; Mosbahi, K.; Kelly, Sharon M.; Byron, O.; Smith, Brian O.;
1038 Walker, D. The Potassium Binding Protein Kbp Is a Cytoplasmic Potassium Sensor. *Structure*
1039 **2016**, *24* (5), 741-749. DOI: 10.1016/j.str.2016.03.017 (accessed 2023/01/13).
1040 (103) Hseiky, A.; Crespo, M.; Kieffer-Jaquinod, S.; Fenaille, F.; Pflieger, D. Small Mass but
1041 Strong Information: Diagnostic Ions Provide Crucial Clues to Correctly Identify Histone Lysine
1042 Modifications. *Proteomes* **2021**, *9* (2). DOI: 10.3390/proteomes9020018 From NLM.
1043 (104) Shogren-Knaak, M. A. Mimicking methylated histones. *ACS Chem Biol* **2007**, *2* (4), 225-
1044 227. DOI: 10.1021/cb700067n.
1045 (105) Simon, M. D.; Chu, F.; Racki, L. R.; de la Cruz, C. C.; Burlingame, A. L.; Panning, B.;
1046 Narlikar, G. J.; Shokat, K. M. The site-specific installation of methyl-lysine analogs into
1047 recombinant histones. *Cell* **2007**, *128* (5), 1003-1012. DOI: 10.1016/j.cell.2006.12.041 From
1048 NLM.
1049
1050

Protein K-trimethylation



?

C[N+](C)(C)CCCCC(N)C(=O)O

MS measurements



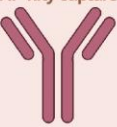
Direct injection



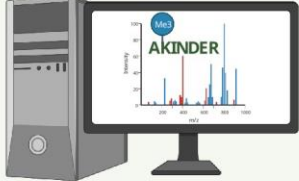
SCX fractionation



Affinity capture



Database searches



Proteome Discoverer



MetaMorpheus



MaxQuant

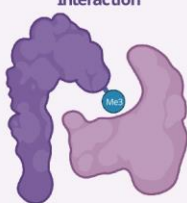


FragPipe



Biological functions

Interaction



Conformation



Active site

